Continental Shelf Research 70 (2013) 13–26

Contents lists available at ScienceDirect

Continental Shelf Research

journal homepage: www.elsevier.com/locate/csr

Research papers

The inner shelf circulation on the Abrolhos Bank, 18°S, Brazil

Carlos E.P. Teixeira [a,*], Guilherme C. Lessa [b], Mauro Cirano [b,c], Carlos A.D. Lentini [b]

[a] Laboratório de Oceanografia Física, Instituto de Ciências do Mar, Universidade Federal do Ceará, Av. Abolição 3207, Fortaleza, CE 60165-081, Brazil
[b] Grupo de Oceanografia Tropical, Instituto de Física, Universidade Federal da Bahia, Brazil
[c] South Australian Research and Development Institute, Australia

ARTICLE INFO

Available online 19 September 2013

Keywords:
Inner-shelf circulation
Abrolhos
Wind-driven circulation
Cold-front systems
Tides

ABSTRACT

The inner shelf circulation on the Abrolhos Bank is investigated using four years (2002–2005) of moored current and bottom pressure observations from two sites in conjunction with wind data from a nearby meteorological station. This is one of the longest projects monitoring current and sea level along the Brazilian coast. The time variability of the local circulation and main forcings are described. For the first time, both the seasonal and the interannual variabilities are addressed, as are the impact of remote forcing. The cross-shore pressure gradient in the region is mostly set up by along-shore winds, whereas the sub-inertial cross-shore momentum balance is essentially geostrophic, with smaller contributions from the cross-shore wind stress. The along-shelf momentum balance is ageostrophic and mainly occurs between the wind and bottom stresses. South-southwestward along-shore currents occur between October and January, whereas stronger north-northeastward currents are observed in fall and winter. This seasonal cycle is driven by the N–S migration of the South Atlantic High between the seasons. An increasing frequency of the southern winds and, consequently, northward currents are observed between 2002 and 2005 and are related to both the number of fronts reaching the region and the remote effect of fronts that did not cross the area. The cross-shore circulation is weak and mainly forced by the tides. It is suggested that long-period shelf waves that propagate into the region change the inner shelf current field and sea level.

1. Introduction

Although the general coastal circulation in southern ($>19°S$) Brazil and around the La Plata River mouth has been reasonably well studied, the coastal circulation north of Rio de Janeiro remains nearly unknown. The circulation of the inner and mid-Brazilian continental shelves has been monitored by a few short-term program, but until the beginning of this century, no current measurements had been performed in the northeastern shelf ($<19°S$). Furthermore, there is no report of monitoring programs for long periods along the Brazilian coast.

The northeastern continental shelf has an average width of 50 km but can reach up to 200 km in front of Caravelas (Fig. 1), where a large coral reef system develops. The reef complex is shallower than 30 m (Leão and Ginsburg, 1997) and is cut by two main channels (~20 km wide and 50 km long), namely, the Canal de Abrolhos and Canal de Sueste (Fig. 1), both with a NE–SW orientation. The water circulation within these channels was initially studied by Leipe et al. (1999) for a week in January 1995. The authors reported a southbound and tide modulated along-shore current within Canal Abrolhos with a mean speed of 0.25 m s^{-1}.

A program to monitor water and suspended-sediment circulation inside Canal de Sueste (Fig. 1) was contracted by the company Aracruz Cellulose to assess the impact of dredging activities on the nearby coral reefs. The monitoring began in January 2002 and was based on the deployment of two current meters. The first 18 months of data were analyzed by Lessa and Cirano (2006), who reported that the large-scale wind field and sub-inertial flows were the most important driving mechanisms for the inner-shelf circulation. The inner and mid-shelf circulations 250 km north of the Abrolhos Bank were also described by Amorim et al. (2011), who used current observations from two seasons to characterize the sub and supra-inertial circulations in this region.

The circulation and the sediment transport within the estuaries adjacent to the Abrolhos Bank are relatively well studied (Schettini and Miranda, 2010; Pereira et al., 2010; Andutta and Miranda, 2013). These studies show in common that the estuaries are well mixed and exhibit a pronounced ebb-dominance of the tidal currents. The estuarine circulation does not change much between dry and wet periods due to the relatively negligible fresh water inflow. Schettini et al. (2013) examined the sediment transport at the Caravelas estuary and showed that the resuspension and settling of the sediments is mostly driven by tidal currents. The

* Corresponding author. Tel.: +55 85 3366 7021.
E-mail address: ocecept@gmail.com (C.E.P. Teixeira).

0278-4343/$ - see front matter © 2013 Elsevier Ltd. All rights reserved.
http://dx.doi.org/10.1016/j.csr.2013.09.003

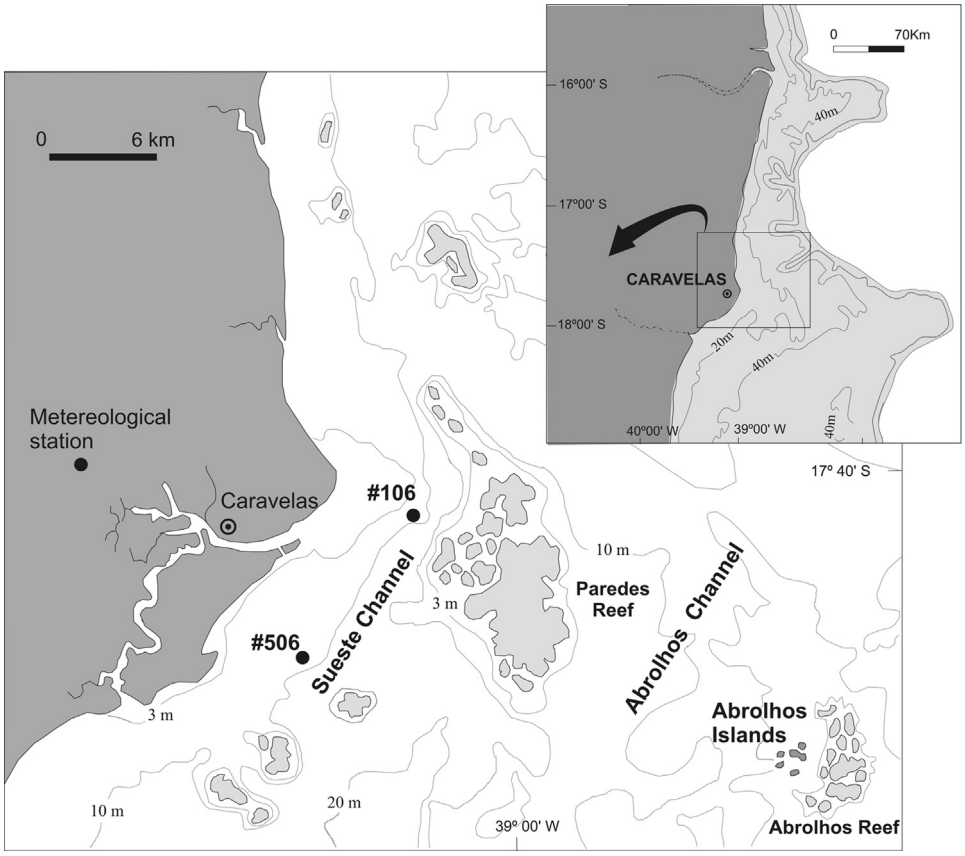

Fig. 1. Location of the study area and the position of the oceanographic and meteorological stations.

authors also observed a persistent net positive water flux in the Caravelas estuary, indicating a dominant mass transport of water and sediment toward the estuary. Nevertheless, the importance of the inner shelf circulation in the sediment transport has not yet been addressed.

The Brazil Current (BC) is the western boundary current flowing southward adjacent to the Abrolhos Bank. There are few numerical modeling and observational studies (Campos, 2006; Soutelino et al., 2011) suggesting that the BC's meso-scale activity produces eddies that reach the shelf region. However, the impact of these eddies in the shelf circulation has also not yet been determined.

In this paper, we expand the statistical analysis performed by Lessa and Cirano (2006) to a time series of four years (2002–2005). For the first time, we investigate both the seasonal and interannual variabilities and the impact of remote forcing on the local sea level and current variability. This is one of the longest current and sea level monitoring programs along the Brazilian coast. The paper is organized as follows: Section 2 describes the dataset and methods used in this study. The results of the main aspects of the winds, sub-inertial and supra-inertial circulations and sea level are presented in Section 3. Cross and along-shore sub-inertial momentum balances are also presented in Section 3. Section 4 presents a discussion of the results. Finally, the main conclusions are given in Section 5.

2. Data and methods

Interocean S4ADW current meters were framed 3 m above the bottom in two locations in the Canal Sueste (stations #106 and #506 in Fig. 1). The instruments were located 14.3 km apart and 9 km offshore. The local water depths were 7.7 m and 8.7 m, respectively. The instruments were configured to record a 2-min average (sampling frequency of 2 Hz) of currents, turbidity and water level every 30 min. To minimize the effects of biofouling, the sites were visited mostly on a weekly basis, when equipment maintenance and data downloads were performed. Spurious values were identified and removed, and the gaps were filled in. Gaps associated with equipment malfunction represented less than 6% of the observations, and those less than 8 h were filled in using a spline interpolator. Hourly sea level data between November 2004 and December 2005 from two stations, Cananéia (~1300 km to the south) and Macaé (~760 km to the south), were also used to investigate the propagation of shelf waves within the study region.

Wind data were provided by a Campbell weather station positioned 12 km inland from the coast (Fig. 1) at an elevation of 114 m. The instrument was configured to record meteorological data every 30 min. The along-shore and cross-shore components of the currents and wind-stress fields were rotated based on the coastline orientation. The along-shore component is positive toward 35°T, and the cross-shore component is positive offshore. To maintain the same reference frame, the wind velocity vectors were rotated a further 180°, meaning northeastern winds (NE) (blowing to the southwest) and onshore winds had negative along-shore and cross-shore components, respectively.

Low-frequency (sub-inertial) components of all datasets were obtained by filtering the data with a 39-h (the inertial period of the location) low-pass Lanczos filter. Harmonic analysis of the tidal currents was performed at sea level and for the along- and cross-shore current components, in accordance with Pawlowicz et al. (2002).

Sea level, wind and current time series were subjected to coherence and power spectral analysis using a 50% overlap and were then detrended and multiplied using a Hanning window of variable size (Emery and Thomson, 1997). White noise was added to the time series to fill in the gaps and allow the analysis of the whole time series. The time variability of the power spectra was

calculated via wavelet spectrum analysis using a Morlet Wavelet transform (Grinsted et al., 2004).

Cross- (x) and along-shore (y) momentum balances were calculated using the x and y components of the shallow-water equations based on the sub-inertial current and wind data.

Monthly climate reports (INPE, 2011) between January 2002 and December 2005 were used to assess the number of cold fronts and upper tropospheric cyclonic vortices (UTCV) that reached the study area.

Table 1
Frequency (%) of wind directions from 2002 to 2005.

	2002	2003	2004	2005	Mean
N	13.5	10.1	9.2	10.3	10.7
NE	25.9	24.9	19.3	23.5	23.3
E	18.4	15.2	12.9	15.1	15.3
SE	12.7	13.9	9.0	13.7	12.2
S	12.0	15.1	21.0	19.6	17.1
SW	7.8	7.0	9.1	9.2	8.3
W	4.0	4.6	2.1	3.2	3.4
NW	4.7	4.8	4.7	4.1	4.6

3. Results

3.1. Winds

A recovery rate of 100% was obtained for the meteorological data. Table 1 shows that the predominant wind direction was NE (mean occurrence of 23.3%). This wind direction was also associated with the highest wind speeds ($>9\ m\ s^{-1}$) measured at this station. Fig. 2 presents the seasonal wind direction and speed for the 4-year period. NE winds were predominant during summer (29% of occurrence), when the mean wind direction was 60° and the average velocity was $4.2\ m\ s^{-1}$. Southeasterly (SE)/south (S)/southwesterly (SW) winds became dominant during the fall and winter (55% and 48% of occurrence, respectively), but the winds had a lower mean velocity of $3.5\ m\ s^{-1}$ and $3.9\ m\ s^{-1}$, respectively. The associated mean wind direction was 151° and 119°,

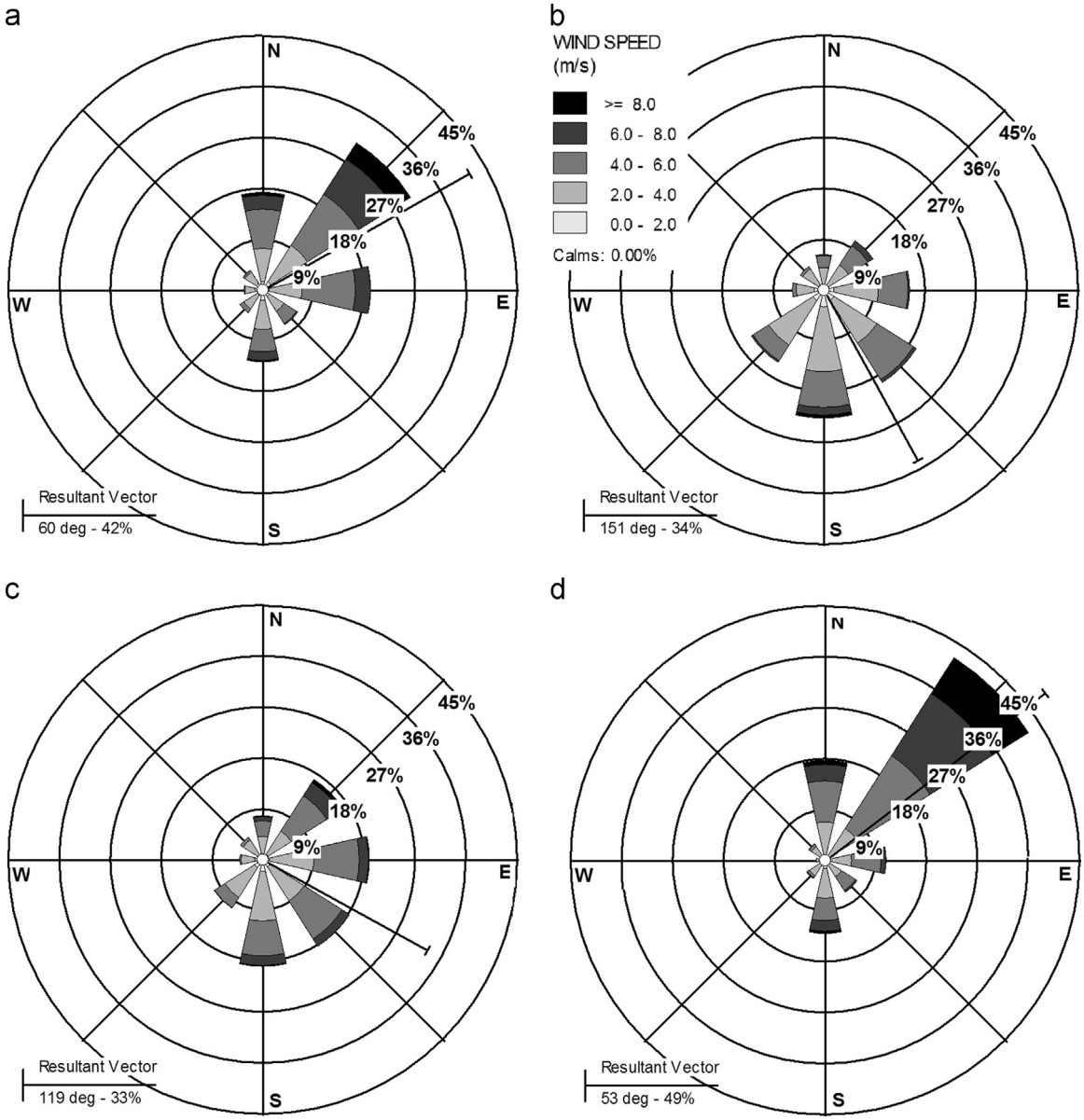

Fig. 2. Mean seasonal wind roses for the data collected between 2002 and 2005 at the meteorological station presented in Fig. 1, representing the following austral seasons: (a) summer, (b) fall, (c) winter and (d) spring.

respectively. The winds rotated again toward the north in spring, when the mean wind direction reached 53°, with an average wind velocity of 4.9 m s^{-1}. This seasonal swing of the wind field was related to the onset (during spring) and waning (during fall) of the trade winds, following the north (N)–south (S) migration of the South Atlantic High between summer and winter (Chaves, 1999).

Significant interannual variations of the wind field were observed, as the mean wind vector shifted 25° eastwards between 2002 and 2005 (not shown). During the 4-year period, the annual mean wind velocities varied by 1.1 m s^{-1} and showed a trend of decreasing values toward 2004, with a small increase in 2005. This direction shift is a consequence of a decrease in the frequency of N and NE winds and an increase in the frequency of S and SW winds (Table 1 and Fig. 3). This trend is ascribed both to a less frequent formation of UTCV over the area and more frequent arrivals of cold fronts (Fig. 3). An even higher increase in the cold front activity between 2002 and 2005 was observed at 23°S (Cabo Frio, 650 km to the south), where the number of events increased from 31 to approximately 40 (Fig. 3). Several of these systems did not reach Caravelas but would have had a remote effect, thus lowering the NE wind velocities farther north.

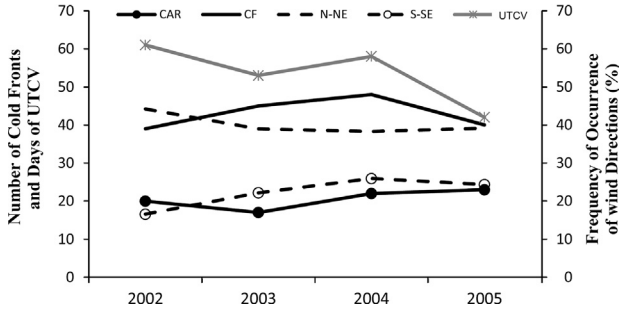

Fig. 3. Number of cold front systems per year that reached Caravelas (CAR) and Cabo Frio (CF) (23°S) and frequency of wind directions at CAR between 2002 and 2005. While the solid lines indicate the number of events that reached CAR and CF in a given year, the dashed lines indicate the percentage of occurrence of N–NE and S–SE winds in a given year. The light gray line presents the number of days per year when the study region was under the influence of upper troposphere cyclonic vortexes (UTCVs). Data for cold front systems and UTCV were obtained from the Brazilian National Institute of Atmospheric Sciences (INPE – http://climanalise.cptec.inpe.br/~rclimanl/boletim/).

3.1.1. *Sub-inertial winds*

The sub-inertial wind field is presented in Fig. 4. The along-shore wind component was always stronger than the cross-shore component, with mean magnitudes of 1.4 ± 2.9 m s^{-1} and 0.9 ± 1.6 m s^{-1}, respectively. The maximum magnitudes for these same components were 8.4 m s^{-1} and 5.9 m s^{-1}, respectively (Fig. 4).

Approximately 66% of the records correspond to negative along-shore winds (blowing from NW/N/NE/E) with an average speed of -3.1 m s^{-1}. Positive along-shore winds (blowing from SE/S/SW/W) had an average speed of 2.0 m s^{-1} and occurred mostly as transient events. The sub-inertial along-shore wind shifted rather abruptly from positive to negative values, but these values swung back more gradually. The sub-inertial cross-shore winds blew mostly from offshore (negative values) (72% of occurrence), with an average speed of -1.7 m s^{-1}.

An annual cycle with an amplitude of ~4.0 m s^{-1} was observed in the along-shore component, where strong negative values during summer, culminating in December, alternated with

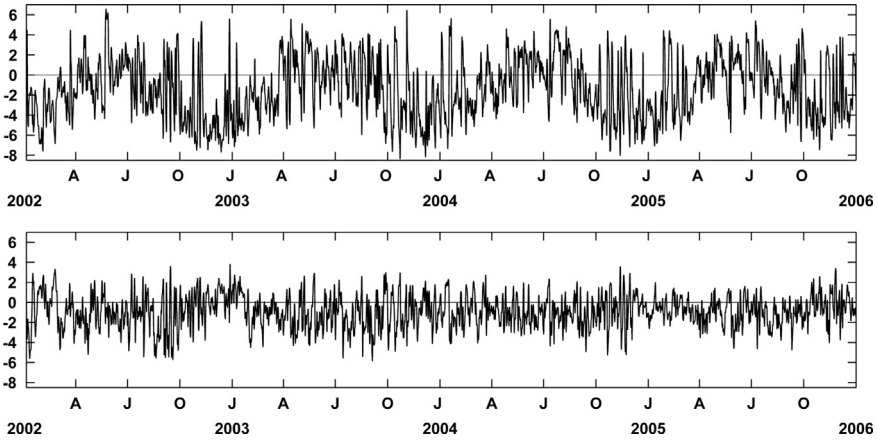

Fig. 4. Time series of the sub-inertial along-shore (upper panel) and cross-shore (lower panel) components of the wind between 2002 and 2005. Positive values of the along-shore (cross-shore) components are associated with SW (from land) winds. Units are m s^{-1}.

Table 2
Annual statistics of the sub-inertial components of the wind field. lower and upper denote the 95% confidence interval for each year. P and N refer to the positive and negative values, respectively, of a given component. The along-shore component is positive NE, and the cross-shore component is positive offshore.

Year	Mean (m s^{-1})	StDev (m s^{-1})	Lower (m s^{-1})	Upper (m s^{-1})	Max P (m s^{-1})	Max N (m s^{-1})	Frequency P (%)	Frequency N (%)
Along-shore wind component								
2002	−2.0	3.0	−2.04	−1.96	6.6	−7.7	25.6	74.4
2003	−1.4	3.0	−1.44	−1.36	6.5	−8.4	33.6	66.4
2004	−1.1	2.9	−1.14	−1.06	5.7	−8.1	36.1	63.9
2005	−1.2	2.8	−1.24	−1.16	5.5	−7.5	37.9	62.1
Cross-shore wind component								
2002	−0.9	1.9	−0.93	−0.87	3.8	−5.7	33.7	66.3
2003	−1.1	1.7	−1.13	−1.07	3.0	−5.6	27.6	72.4
2004	−0.9	1.5	−0.92	−0.88	3.6	−5.3	25.7	74.3
2005	−0.8	1.3	−0.82	−0.78	3.4	−4.8	25.5	74.5

lighter positive values, mostly between May and July (Fig. 4). No clear seasonality was observed in the cross-shore component.

The mean annual along-shore wind speed was negative for all years (Table 2) but showed a trend of decreasing values that was associated with more frequent, but overall weaker, positive along-shore winds. Curiously, although the annual frequency of negative along-shore winds decreased along the years, its respective wind speed increased. Cross-shore winds, in comparison, varied little over the years, with no observable trend except an increase (decrease) in the frequency of the negative (positive) winds (Table 2).

The Fourier spectral analysis of the sub-inertial along-shore winds (Fig. 5) shows stronger cycles with 12-, 16- (highest) and 22-day periods. These cycles bundle together in the output of the wavelet analysis (not presented). It is observed that most of the energy in these frequencies was concentrated within periods of 1–2 months, normally between June and November, although not regularly in all years. The energy peaks at 8 and 74 days in Fig. 5 are also observed in the wavelet analysis. Whereas the former occurred regularly throughout the years, the latter was observed in only four occasions, both in summer and in winter.

3.2. Currents

Recovery rates of 91% and 94% were obtained for stations #106 and #506, respectively. The average current velocity magnitude was 0.18 ± 0.10 m s^{-1} at #506 and 0.25 ± 0.14 m s^{-1} at #106, with maximum values of 0.66 m s^{-1} and 0.93 m s^{-1} in these respective stations. Stronger flows at #106 are ascribed to its narrower cross-section geometry (Fig. 1). Fig. 6 shows that the directions of the currents, mainly at #106, tend to follow a bimodal distribution, although the wider cross-section at #506 allows for the establishment of other flow directions (mainly E, W and NW).

The harmonic analyses of the rotated currents indicate that the diurnal tidal ellipses were approximately transverse to the coastline in both stations (Table 3). The semi-diurnal ellipses were, conversely, more parallel to the orientation of the coastline, deviating by 41° at station #106 and 58° at station #506. The maximum amplitude of the M_2 component was 0.16 m s^{-1} at station #106.

The reconstituted tidal currents explain 35.3% of the total current variance recorded at station #106, with the cross-shore (along-shore) component explaining 70.8% (28.3%) of the variance. The maximum tidal current magnitude at station #106 was 0.43 m s^{-1} in the along-shore direction and 0.21 m s^{-1} in the cross-shore direction.

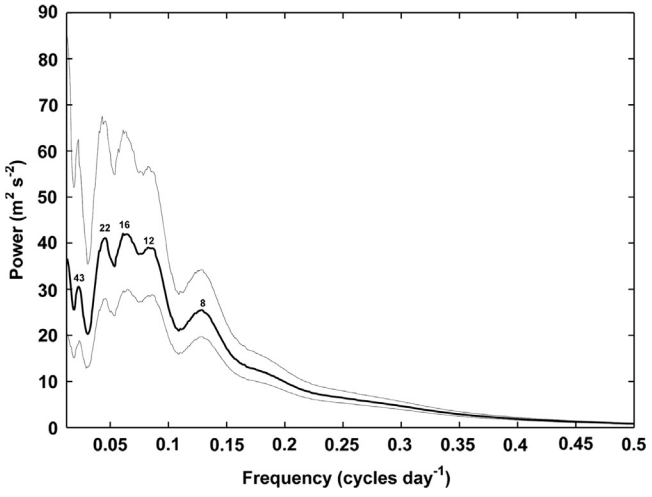

Fig. 5. Fourier power spectrum of the sub-inertial along-shore component of the wind between 2002 and 2005 in Caravelas. Numbers shown in the plot represent the associated period for the relevant peaks (days). The upper and lower gray lines represent the 95% confidence spectrum.

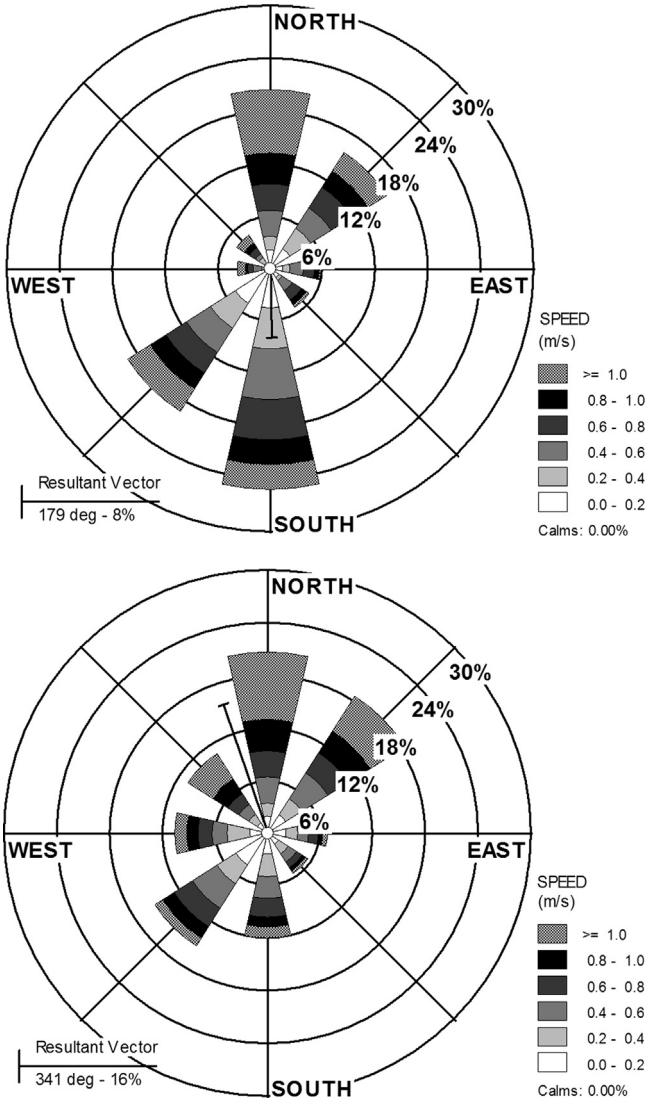

Fig. 6. Frequency of occurrence of current direction and velocity between January 2002 and December 2005 for stations #106 (upper panel) and #506 (lower panel).

In the less channelized position of station #506, the reconstituted tidal currents explained 39.9% of the total current variance, again explaining more of the cross-shore (67.7%) than the along-shore (29.8%) variance. The maximum tidal current magnitude at station #506 was 0.30 m s^{-1} in the along-shore direction and 0.22 m s^{-1} in the cross-shore direction.

3.2.1. Sub-inertial currents

In the sub-inertial band, the along-shore currents had a mean magnitude of 0.10 ± 0.21 m s^{-1} at station #106 (Fig. 7) and 0.04 ± 0.14 m s^{-1} at station #506 (Fig. 8). Maximum values for the along-shore component were recorded in September 2002 as -0.72 m s^{-1} and 0.49 m s^{-1}, respectively, at these same stations. The sub-inertial band explains 74% (#106) and 68% (#506) of the total along-shore current variance, respectively. Sub-inertial cross-shore (v) currents were much weaker, with mean magnitudes of 0.01 ± 0.05 m s^{-1} for both stations. The maximum values for this component were 0.20 m s^{-1} at those stations. The sub-inertial band explains 23% (#106) and 22% (#506) of the total cross-shore current variance.

The monthly mean values for the sub-inertial along-shore currents are plotted in Fig. 9. A seasonal cycle in the along-shore

Table 3
Harmonic components of the tidal currents for stations #106 and #506. The inclinations refer to True North and phases, relative to Greenwich. Errors are the 95% confidence interval estimates.

Component	Major ($m\,s^{-1}$)	Error	Minor ($m\,s^{-1}$)	Error	Inclination (°)	Error	Phase (°)	Error
Station #106								
M_2	0.16	0.003	−0.067	0.01	41	1.1	171	1.0
S_2	0.08	0.003	−0.027	0.01	36	1.8	176	1.8
O_1	0.04	0.003	−0.003	0.00	5	2.0	315	4.4
K_1	0.02	0.003	0.001	0.00	3	3.7	335	7.7
Station #5p06								
M_2	0.11	0.002	−0.091	0.01	58	3.4	169	3.5
S_2	0.06	0.002	−0.037	0.01	45	3.6	162	3.5
O_1	0.02	0.003	−0.003	0.00	1	3.8	286	6.7
K_1	0.02	0.003	0.003	0.00	179	4.5	135	8.0

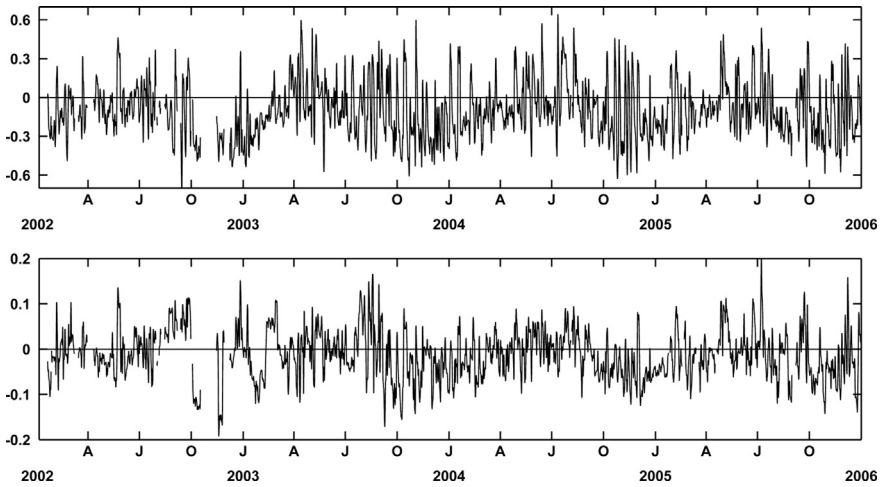

Fig. 7. Time series of the sub-inertial along-shore (upper panel) and cross-shore (lower panel) components of the currents at station #106 between 2002 and 2005. The panels have different scales along the *y*-axis. Units are $m\,s^{-1}$.

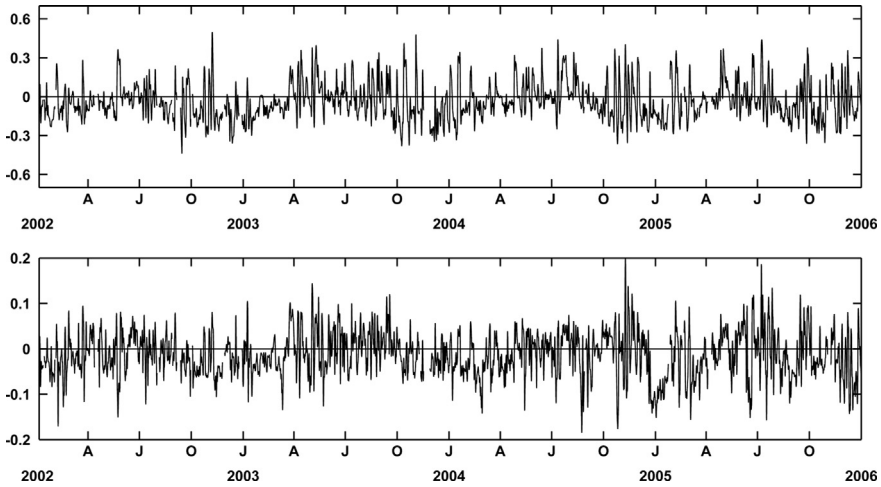

Fig. 8. Time series of the sub-inertial along-shore (upper panel) and cross-shore (lower panel) components of the currents at station #506 between 2002 and 2005. The panels have different scales in the *y*-axis. Units are $m\,s^{-1}$.

currents is clearly observed with oscillations of $0.40\,m\,s^{-1}$ and $0.20\,m\,s^{-1}$ at stations #106 and #506, respectively. Stronger negative (southward currents) along-shore currents occurred between October and January, when the maximum absolute values reached $-0.35\,m\,s^{-1}$ and $-0.15\,m\,s^{-1}$ at stations #106 and #506, respectively. Stronger positive (northward) along-shore currents are observed in the fall and winter months, when maximum values of $0.07\,m\,s^{-1}$ at station #106 and $0.08\,m\,s^{-1}$ at station #506 were recorded. A notable aspect in Fig. 9 is the decrease of the maximum monthly mean negative velocity along the years, from $-0.35\,m\,s^{-1}$ in 2002 to $-0.20\,m\,s^{-1}$ in 2004 and 2005, a trend similar to that observed in the wind field. Harmonic analysis shows that the annual cycle explains 59% and 54% of the total variance of the along-shore currents at stations #106 and #506, respectively.

In the cross-shore direction (Figs. 7 and 8, lower panel), offshore-oriented currents tend to occur in fall, while onshore

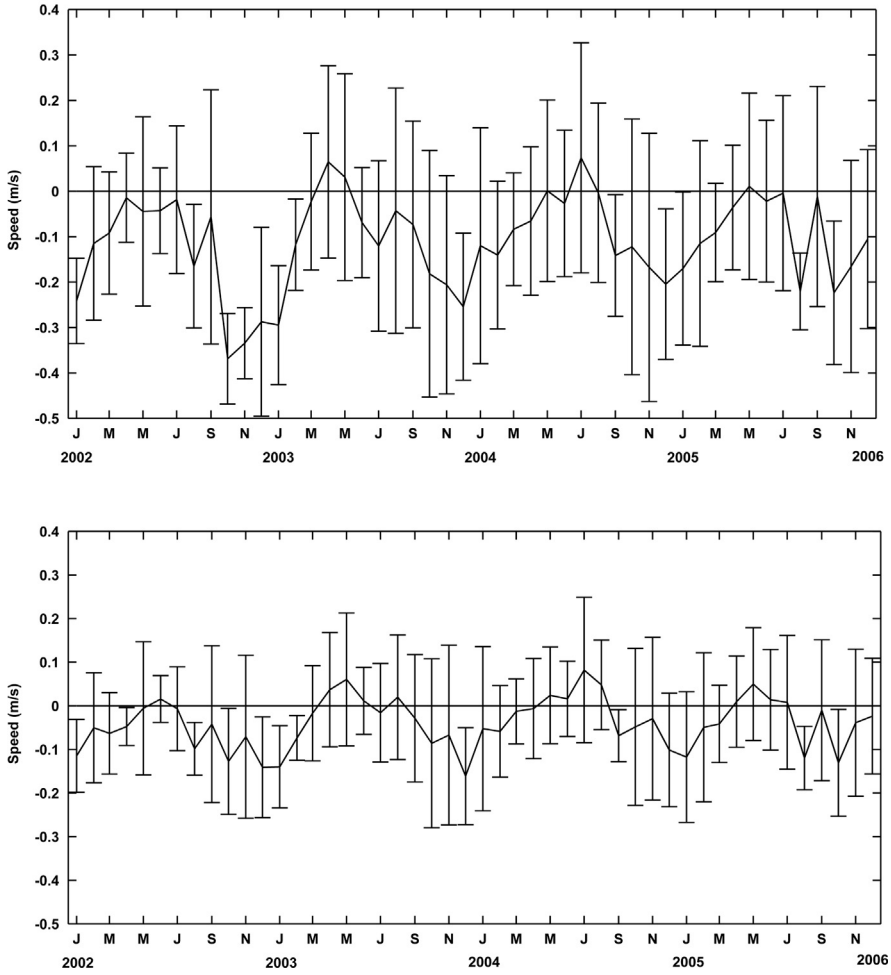

Fig. 9. Time series of the monthly mean along-shore components of currents at stations #106 (upper panel) and #506 (lower panel) between 2002 and 2005. The vertical bars represent the standard deviation.

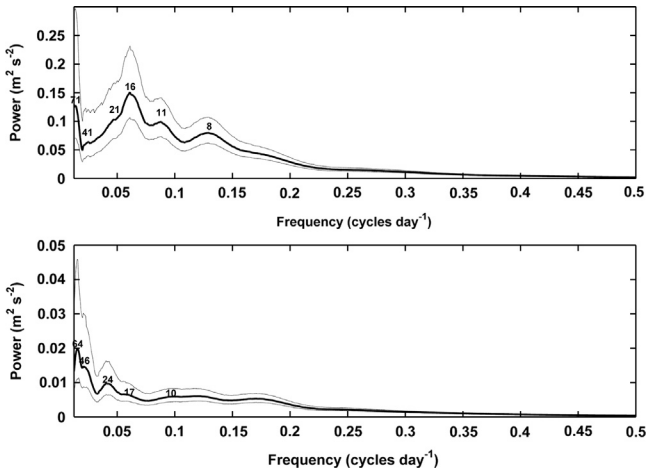

Fig. 10. Fourier power spectrum of the sub-inertial along-shore (upper panel) and cross-shore (lower panel) currents at station #506 between 2002 and 2005. The numbers shown in the plot represent the associated period for the relevant peaks (days). The upper and lower gray lines represent the 95% confidence spectrum.

oriented currents prevailed in summer. The seasonal pattern, however, was less conspicuous than that of the along-shore currents, with oscillations of 0.10 m s^{-1} at station #106 (Fig. 7) and 0.07 m s^{-1} at station #506 (Fig. 9). Harmonic analysis shows that the annual cycle explains 32% and 41% of the total variance of the cross-shore currents at stations #106 and #506, respectively.

The spectral analysis of the sub-inertial along-shore current at station #506 (Fig. 10) shows stronger cycles at periods of 11, 16 (highest) and 71 days. The 11- and 16-day cycles, along with a subordinate 8-day cycle, are close to those observed in the wind field spectra. The cross-shore current spectrum shows a relatively high energy concentration at 64 and 24 days. Wavelet analysis for the along-shore currents (not presented) shows that most of the variability occurred between 4 and 45 days. The results also indicate that the energy during those periods, as highlighted by the spectral analysis, is not evenly distributed along the years. The 64-day cycles are mainly associated with an event that took place in the second semester of 2005. The wavelet analysis for the cross-shore currents (not presented) also indicates that the most energetic periods were related to the 4- to 45-days band and were not uniformly distributed along time. Compared with the along-shore currents, the periods of variability higher than 8 days were less frequent.

The spectral and wavelet results from both stations were very similar, and only the results from station #506, which had the best recovery rates, are presented.

3.3. Sea level

Recovery rates of 88% and 94% were obtained for stations #106 and #506, respectively. Because the sea level records from both stations were nearly identical (R^2=0.98), only the data from

station #506, which is the location with the best recovery rates, are presented.

The tides are semi-diurnal, with a form number of 0.14 and heights that range from a minimum of 0.47 m (neap tide) to a maximum of 3.39 m (spring tide). A list of the harmonic components (Table 4) shows that the amplitudes of the largest semi-diurnal harmonic components (M_2 and S_2) were 0.9 m and 0.38 m, respectively. The reconstituted (or astronomical) tidal signal explains 97% of the sea level variability.

3.3.1. Sub-inertial sea-level

The monthly mean sea level presented in Fig. 11 shows a seasonal cycle with positive values occurring during the fall and winter months. While the sub-inertial sea level oscillations had a mean amplitude of 0.22 m, the largest sub-inertial oscillation was 0.45 m in July 2005, associated with SE wind speeds of 7.5 m s^{-1}. Harmonic analyses show that the annual cycle explains 37% of the total annual variance of the sea level.

The spectral analysis of the sub-inertial sea level oscillations at station #506 shows two main energy peaks situated at periods of 16 and 72 h (Fig. 12). The sea-level wavelet results (not presented) show that the most energetic periods are related to the 4- to 16-days band. Compared with the results for the sub-inertial currents and wind, the energy is more sparsely distributed, with several gaps that encompass all period ranges. Most of these gaps tend to occur between January and April.

Table 4
Main harmonic components of the sea level at station #506. Errors are the 95% confidence interval estimates.

Component	Amplitude		Phase	
	(m)	Error	(°)	Error
M_2	0.90	0.004	99	0.2
S_2	0.38	0.004	114	0.6
O_1	0.09	0.002	110	1.3
K_1	0.05	0.002	177	2.2
M_4	0.04	0.002	253	3.4
N_2	0.15	0.004	101	1.5
K_2	0.11	0.004	106	1.8
MN_4	0.03	0.002	216	4.9
$2MS_6$	0.01	0.001	242	6.4
P_1	0.02	0.002	172	5.7

3.4. Momentum balance

Cross- (x) and along-shore (y) momentum balances were calculated using the x and y components of the shallow-water equations:

$$\underbrace{\frac{\partial \overline{u}}{\partial t}}_{\text{ACX}} \underbrace{-f\overline{v}}_{\text{CFX}} + g\underbrace{\frac{\partial \eta}{\partial x}}_{\text{PGX}} - \underbrace{\frac{\tau_x^s}{\rho_0 H}}_{\text{WSX}} + \underbrace{\frac{\tau_x^s}{\rho_0 H}}_{\text{BSX}} + \underbrace{OT_X}_{\text{OTX}} = 0 \quad (1)$$

$$\underbrace{\frac{\partial \overline{v}}{\partial t}}_{\text{ATY}} + \underbrace{f\overline{u}}_{\text{CFY}} + g\underbrace{\frac{\partial \eta}{\partial y}}_{\text{PGY}} - \underbrace{\frac{\tau_y^s}{\rho_0 H}}_{\text{WSY}} + \underbrace{\frac{\tau_y^b}{\rho_0 H}}_{\text{BSY}} + \underbrace{OT_Y}_{\text{OTY}} = 0 \quad (2)$$

where x and y denote the cross- and along-shore directions, respectively, with x being positive offshore and y being positive northeastward; (u, v) are velocity components; f is the Coriolis parameter; g is the gravitational acceleration; ρ_0 is a reference density; $(\partial\eta/\partial x, \partial\eta/\partial y)$ are the pressure gradients due to the sea level (η) oscillations; H is the total water depth ($h+\eta$); and (τ_x^s, τ_y^s) and (τ_x^b, τ_y^b) are the surface and bottom stresses, respectively. The terms are associated with the local acceleration (ACX, ACY), the Coriolis acceleration (CFX, CFY), the pressure gradient (PGX, PGY), the wind stress (WSX, WSY) and the bottom stress (BSX, BSY).

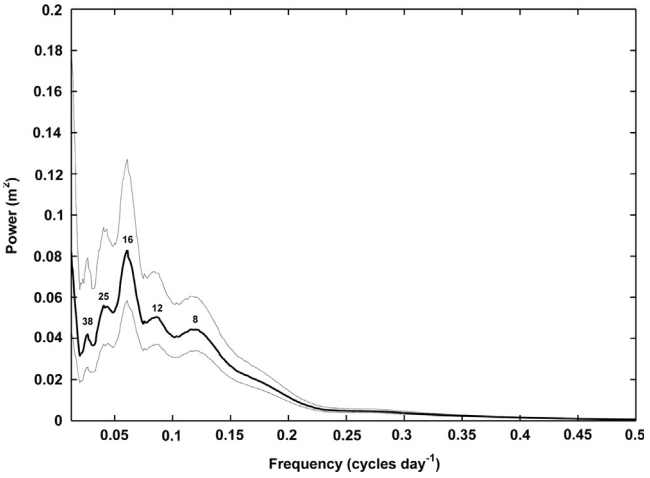

Fig. 12. Fourier power spectrum of the sub-inertial sea level oscillations at station #506 between 2002 and 2005. The numbers shown in the plot represent the associated period for the relevant peaks (days). The upper and lower gray lines represent the 95% confidence spectrum.

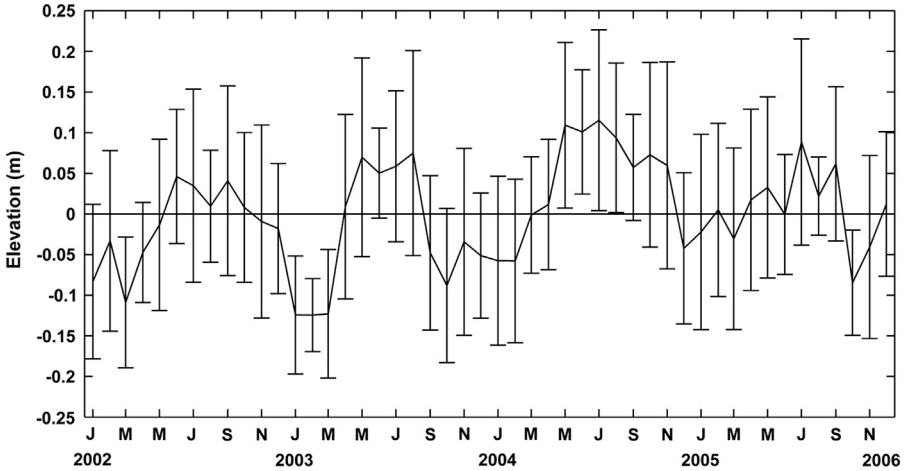

Fig. 11. Time series of the monthly mean sea level elevation at station #506 from 2002 to 2005. The vertical bars represent the standard deviation.

The remaining terms were named "other terms" (OTX, OTY) and represent the terms that match the estimated momentum balance for each component. Therefore, the OTX and OTY terms are associated with the terms that are neglected here (e.g., non-linear horizontal advection, lateral friction) plus a residual. The residual may be ascribed to observational and diagnostic errors and to the simplified dynamics (Liu and Weisberg, 2005).

The local acceleration and pressure gradient terms were computed through forward difference. The wind stress term was estimated using a neutral drag law (Large and Pond, 1981). Following Liu and Weisberg (2005), the cross- and along-shore bottom stress terms were estimated in different ways. The cross-shore component of the bottom stress was parameterized by the quadratic form $\tau_x^s = \rho_0 C d \bar{u} (\bar{u}^2 + \bar{v}^2)^{1/2}$, where Cd is a drag coefficient taken to be 2.5×10^{-3}. The along-shore component of the bottom stress was parameterized using a linear form, $\tau_y^b = \rho_0 r \bar{v}$, where r is a resistance coefficient taken to be 2.5×10^{-4}. Different values for Cd and r were tested; however, the values presented above resulted in smaller residual terms and higher correlation and regression between the terms. The components of the velocity measured at a depth of 3 m above the bottom were considered an approximation of the water column velocity.

Because stations #106 and #506 were nearly aligned in the cross-shore direction, the pressure gradient was estimated by

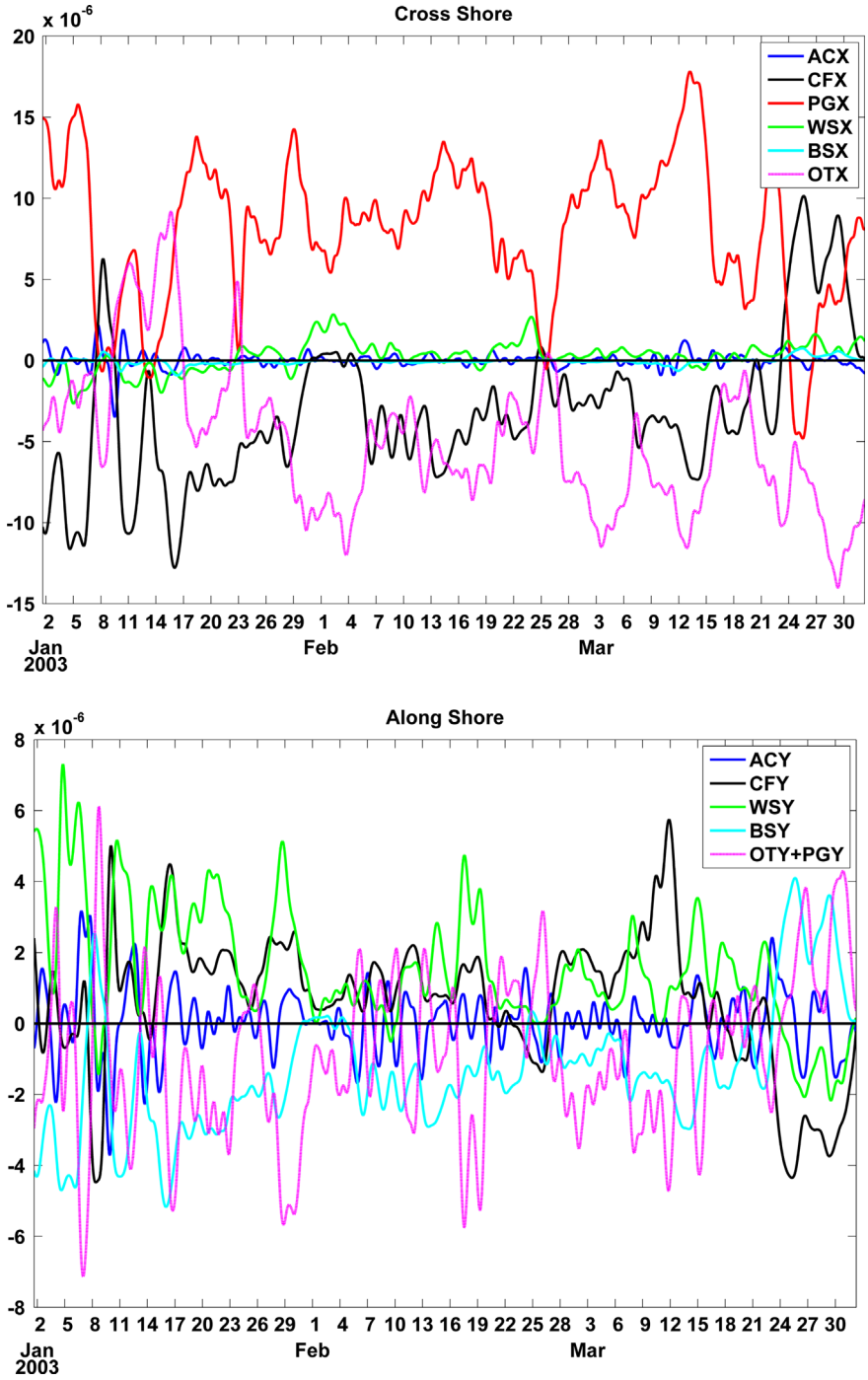

Fig. 13. Vertically integrated cross (upper panel) and along-shore (lower panel) momentum balance (units in 10^{-6} m s^{-2}) for the #506 station.

Table 5
Term estimates of the cross and along-shore momentum balance (units in 10^{-6} m s^{-2}) for the #506 station, as defined in Eqs. (1) and (2).

	ACX	CFX	SGX	WSX	BSX	OTX
Cross-shore						
Mean	0.00	−3.23	8.04	0.24	−0.05	−5.00
Standard deviation	0.49	4.37	4.39	0.91	0.22	4.27
	ACY	CFY	SGY	WSY	BSY	OTY+PGY
Along-shore						
Mean	0.03	0.65	–	−1.54	1.31	1.98
Standard deviation	0.92	1.84	–	1.71	1.76	2.2

Local acceleration (ACX, ACY), coriolis acceleration (CFX, CFY), pressure gradient (PGX, PGY), wind stress (WSX, WSY), bottom stress (BSX, BSY) and other terms (OTX, OTY).

assuming that the sea level equals zero at the shelf break located 180 km offshore. The pressure gradient in the along-shore direction was not considered because unrealistic values were found, most likely because the sea level sensors at #106 and #506 were separated by only 14 km. In the along-shore direction, therefore, the OTY plus the pressure gradient was considered a single term.

The momentum balances were calculated using the sub-inertial data from station #506 during the period between January and March 2003. This is the best quality and the longest period without gaps for both stations.

3.4.1. The cross-shore momentum balance

The time series of the cross-shore momentum terms (Fig. 13) shows that the Coriolis and pressure gradients are the largest terms, suggesting that the cross-shore momentum balance is predominantly geostrophic. This conclusion is supported by the relative magnitude of each term, estimated by the mean and standard deviations (Table 5). The remaining terms, of diminishing importance, are the wind stress, the local acceleration and the bottom stress. While the wind stress term is the third most important term in the balance, it represents only 21% of the standard deviation of the Coriolis term, with both the bottom friction and the local acceleration terms being an order of magnitude smaller than the Coriolis and pressure gradient terms. Although the OTX term has a standard deviation smaller than the leading terms, it still presents significant values. This result is expected because this term incorporated all of the approximations involved in this first-order balance plus the terms that were neglected in our calculations.

The contribution of each term to the momentum balance was estimated using correlation and regression coefficients between the pressure gradient term and the sums of the other terms that were calculated using the full-length records at station #506. The correlation squared coefficient (r^2) and regression (significant at the 95% confidence level) values between the pressure gradient and Coriolis terms are 0.57 and 0.45, respectively. When the wind stress is included, the r^2 and the regression increase to 0.61 and 0.47, respectively. Finally, when the bottom stress is included, the r^2 and the regression increase to 0.64 and 0.48, respectively. No differences were found when the local acceleration term was included in the analysis.

Based on the above results, the depth-averaged along-shore velocity can be expressed as follows:

$$\overline{v} = \frac{1}{f}\left(g\frac{\partial \eta}{\partial x} - \frac{\tau_x^s}{\rho_0 H}\right)$$

The r^2 and the regression between the along-shore currents estimated using this model and the currents measured at station #506 are 0.54 and 0.77, respectively, showing that the cross-shore pressure gradient plus the wind stress are good estimators of the sub-inertial along-shore velocities.

3.4.2. The along-shore momentum balance

While there is visually a balance between the wind and bottom stresses in the along-shore direction of the momentum balance (Fig. 13), the mean and standard deviations of the along-shore momentum terms from station #506 show that the OTY plus the pressure gradient is the largest (Table 5), followed by the wind stress, bottom stress, Coriolis terms and the local acceleration. Except for the local acceleration term, all terms have the same order of magnitude.

The contribution of each term to the momentum balance was estimated using correlation and regression coefficients between the wind stress term and the sums of the other terms using the full-length records at station #506. The values of the r^2 and regression (significant at the 95% confidence level) between the wind stress and the bottom stress terms are 0.76 and 0.90, respectively. When the Coriolis term is included, the correlation does not change and the regression decreases to 0.46. Finally, when the local acceleration is included, the r^2 and the regression increase to 0.72 and 0.47, respectively.

Based on the above results, the depth-averaged along-shore velocity can be expressed as follows:

$$\overline{u} = \frac{1}{f}\left[\frac{\tau_y^s}{\rho_0 H} - \frac{\tau_y^b}{\rho_0 H}\right]$$

The r^2 and the regression between the cross-shore currents estimated using this model and those measured at station #506 are 0.22 and 0.67, respectively, show that the wind and bottom stresses can only explain part of the variability of the sub-inertial cross-shore velocities. This result is expected because the along-shore pressure gradient is not included in our calculations.

4. Discussion

The tidal range in the Abrolhos's inner shelf is the largest open-ocean range along the Brazilian East Coast (5°S–34°S) (Lessa and Cirano 2006). In accordance with Pereira et al. (2005), the tidal amplitudes grow by a factor of 1.5 between the edge of the continental shelf and the inner shelf. This amplification could be ascribed to the geomorphological characteristics of the shelf with shallow reefs and NE–SW-aligned channels (Fig. 1), which are likely to create tidal convergence in the inner shelf fronting Caravelas as the tidal wave enters the region via the northern and southern channel entrances. A similar process, although larger in scale, is responsible for the macrotidal conditions observed behind the Great Barrier Reef in northeast Australia (Griffin et al., 1987).

Despite the significant tidal range and the constriction exerted on the flow by the coral constructions, tidal currents explained only approximately 30% of the total along-shore current variance. The cross-shore circulation, however, was mostly tidally driven, with tidal currents explaining close to 70% of the cross-shore current variance. These results are supported by Amorim et al.

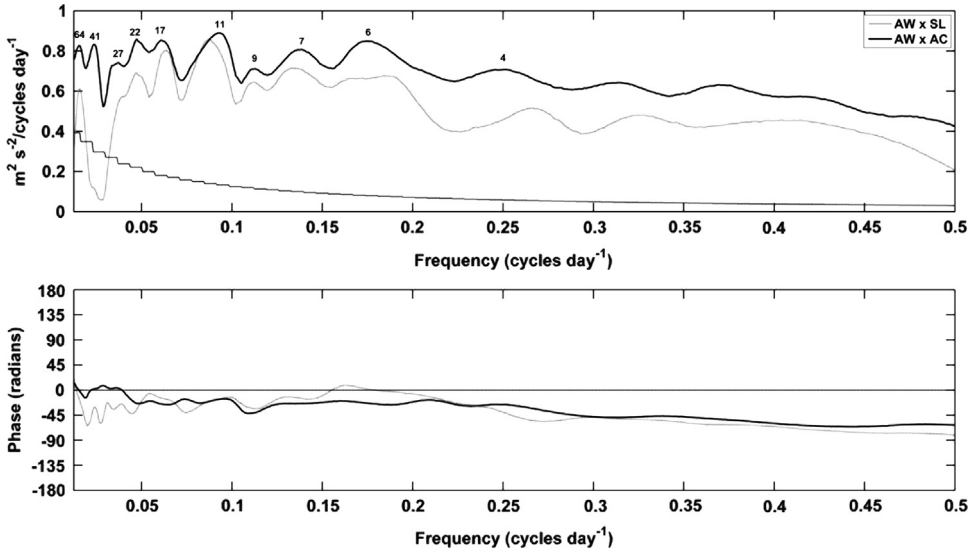

Fig. 14. Cross spectrum and phase lag between the sub-inertial along-shore component of the wind (AW) and sea level at station #506 (SL) (gray line) and between the sub-inertial AW and the along-shore component of the current at station #506 (AC) (black line). The dotted line in the upper panel indicates the 95% confidence interval. The numbers in the upper panel represent the associated period for the relevant peaks.

(2011), who found that the along-shore inner shelf circulation close to Camamu Bay (~400 km to the north) was mostly driven by sub-inertial forcings, while the cross-shore velocity was mainly driven by supra-inertial forcings.

The wind shear and associated pressure gradients were the overriding drivers of the water circulation in the inner shelf. The sub-inertial sea level oscillations were well explained by the along-shore wind field, with a r^2 of 0.5 with no time lag and 0.57 with a 5-h time lag. The coherence spectra between along-shore winds and sea level (Fig. 14) show that the coherences are significant for all frequencies between 0.5 cpd (2 days) and 0.04 cpd (25 days) as well as for frequencies near 0.015 cpd (64 days). High levels of coherence are observed at approximately 11, 17 and 22 days, which may reflect the influence of the cold-front systems. As expected, the along-shore wind spectra showed a negative phase relative to the sea level (the wind field leading the sea level) for all significant frequencies, except those near 0.16 cpd (6 days). The positive phases, however, have no physical explanation because the wind stress is the driving force for the sea level and current variability.

The sub-inertial wind field was also the overriding factor in the determination of the sub-inertial currents. The r^2 between the sub-inertial along-shore components of the wind and currents were 0.59 and 0.62 for stations #106 and #506, respectively. However, these values could be as high as 0.67 at #106, associated with a time lag of 2.5 h, and 0.74 at #506, with a time lag of 4 h. The highest r^2 between the cross-shore currents and along-shore winds was 0.33 at station #106 and 0.36 at station #506, both with a time lag of 4 h.

The r^2 between the sub-inertial along-shore currents and sea level were 0.31 and 0.33 for stations #106 and #506, respectively. The r^2 between the sub-inertial cross-shore currents and sea level was 0.11 for station #106 and 0.16 for station #506.

The coherence spectra between the along-shore winds and currents (Fig. 14) show the coherences are significant for all frequencies below 0.5 cpd (2 days). High coherences were observed at approximately 6, 7, 11, 17, 22, 41 and 64 days. The along-shore wind spectrum showed a negative phase relative to the along-shore current for all significant frequencies.

The statistical results above are supported by the momentum balances in the cross-shore and along-shore directions, which are geostrophic and ageostrophic, respectively. Positive (negative) along-shore winds (blowing from SW/S/SE) induce an onshore (offshore) Ekman transport and water level set up (set down) by the coast. The pressure gradient produced is balanced by the Coriolis acceleration and induces currents in the along-shore direction.

These results agree with previous studies (e.g., Lentz, 1994; Liu and Weisberg, 2005) for the inner shelf along the southeastern USA coast, where the Ekman dynamic is similar to that on the east coast of South America (e.g., storms are associated with equatorward winds, which favor downwelling). Liu and Weisberg (2005) used a momentum balance analysis to show that the along-shore circulation on the inner West Florida Shelf is primarily driven by the balance between the along-shore wind and bottom stress terms, complemented by the pressure gradient, Coriolis and local acceleration terms. Lentz et al. (1999) used four months of moored current, pressure, temperature, conductivity, wave and wind observations on the North Carolina shelf to find the momentum balance over the inner shelf. Similar to our results, the authors concluded that the along-shore momentum balance at this region of the shelf predominantly occurs between the wind and bottom stresses. Similar to our results, both studies also suggested that the cross-shore momentum balance is mainly driven by the pressure gradient and Coriolis. Similar to our results, Liu and Weisberg (2005) showed that the cross-shore wind stress has secondary importance in the cross-shore balance. However, Lentz et al. (1999) showed that the wave setup is more important than the cross-shore wind stress to the balance in this direction. We believe that the wave effect on the pressure gradient should be minor in Caravelas due to the low wave energy characteristic of regions sheltered by a reef system.

The characteristics of the wind field in Caravelas (Fig. 2) point to a relatively lower activity of the southern winds. Although less frequent than the NE winds, their magnitude is normally higher, which is not observed in the wind data from Caravelas. Wind data collected at 6-h intervals at a Navy meteorological station at Abrolhos Island (60 km offshore) between 1957 and 1997 show that the strongest winds are in fact associated with a southern direction. Compared with Abrolhos, the records of the southern winds from Caravelas are biased in terms of both frequency and speed. Therefore, the trend of increasing southern wind frequency between 2002 and 2005, as indicated by the Caravelas data, may have been stronger than anticipated.

The increasing frequency of the southern winds could be caused both by the arrival or proximity of low-pressure systems

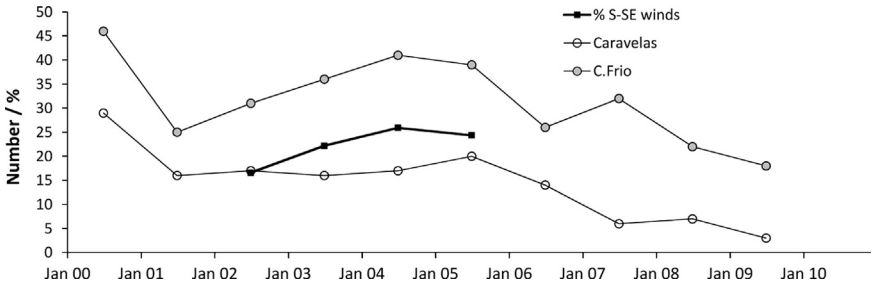

Fig. 15. Time series of the percentage of occurrence of S–SE winds in Caravelas and the number of cold fronts arriving in Caravelas and Cabo Frio (23°S) during the whole year as presented in INPE (2011).

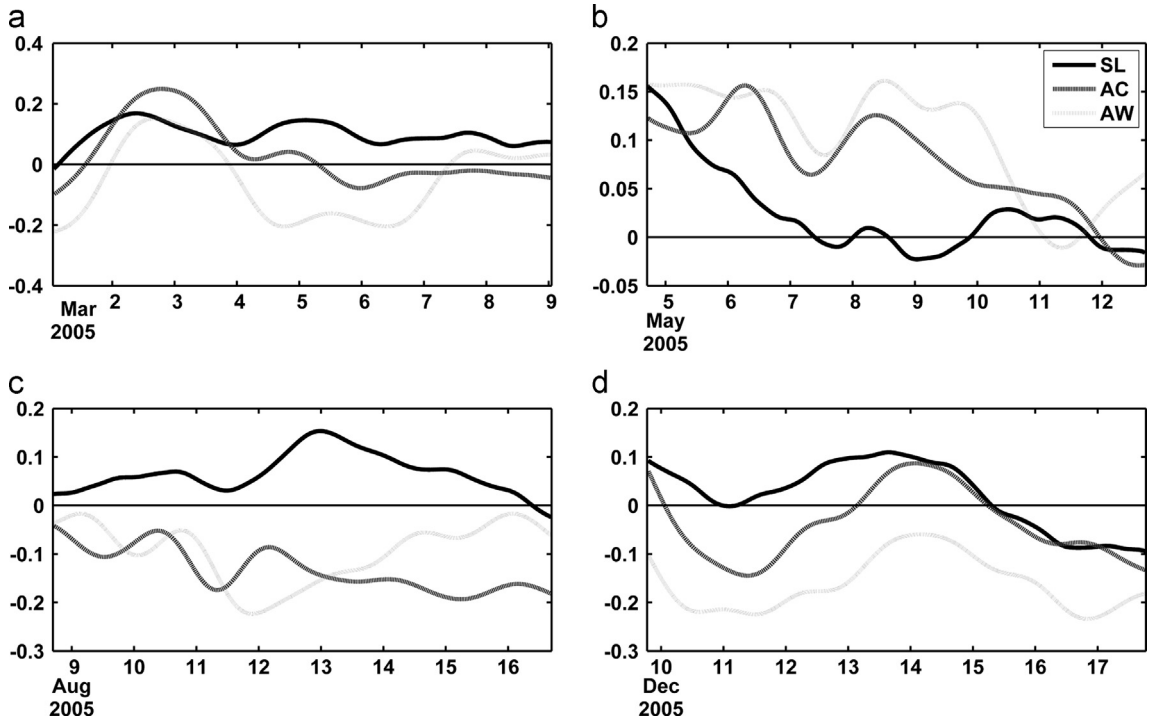

Fig. 16. Sub-inertial along-shore current (AC) and sea level (SL) at station #506 and along-shore winds (AW) on four occasions when sea-level behavior is not explained by the expected wind-driven Ekman response. See text for details. The along-shore wind speed is divided by 20. Velocity scales are different among the plots. Units are m s^{-1} for AC and AW. Units are m for SL.

in the area. Fig. 15a shows that while the number of cold fronts arriving in Caravelas was somewhat stable between 2002 and 2004, the S–SE winds were more frequent and the number of cold fronts reaching the Southeast Brazil (Cabo Frio 23°S) increased. The trend observed in the number of cold fronts reaching SE Brazil between 2002 and 2005 mirrors the trend in the frequency of S–SE winds in Caravelas, indicating that although these systems did not reach the study region they remotely affected the atmospheric circulation. This phenomenon is characteristic of El Niño years, when subtropical cyclones are held over South and Southeast Brazil (Pezza and Ambrizzi, 2003). The Southern Oscillation Index (Australian Bureau of Meteorology – http://www.bom.gov.au/climate/glossary/soi.shtml) and the Oceanic Niño Index for Niño 3.4 region (NOAA – http://www.cpc.ncep.noaa.gov/products/analysis_monitoring/ensostuff/ensoyears.shtml) indicate El Niño conditions between 2002 and 2004, explaining the arresting of low-pressure systems over Southeast Brazil.

The sub-inertial along-shore wind field did not fully explain the variability observed in the sub-inertial sea level and currents. Castro and Lee (1995) showed that sub-inertial sea level oscillations along the SE Brazilian coast were better correlated with winds monitored earlier and farther south than with the local wind at the time of the sea level measurement. Likewise, Rahy (2006), when studying the propagation of shelf waves in the same area, noted that the wind field recorded at a station to the south (~300 km) of Cabo Frio (23°S) had a higher covariance with the measured inner shelf along-shore current than the local wind field. This finding means that a significant part of the observed variability in sea level and currents can be ascribed to a remote wind field that is not exactly similar to the one locally monitored.

It is also likely that the non-explained along-shore current and sea-level variability can be associated with long-period shelf waves set off by low-pressure systems that did not propagate this far north. Such remote control of the sub-inertial hydrodynamics is especially relevant in lower latitudes less frequently visited by atmospheric lows. Fig. 16 shows four selected occasions when the sea level was in disagreement with the wind direction and Ekman transport. Negative along-shore winds (blowing from N/NE/E) are associated with positive mean sea levels in Fig. 16a, c, and d and positive along-shore winds (blowing from SE/S/W) occur simultaneously with falling and negative mean sea levels in Fig. 16b. The coastal current on these four occasions is manly wind driven, but

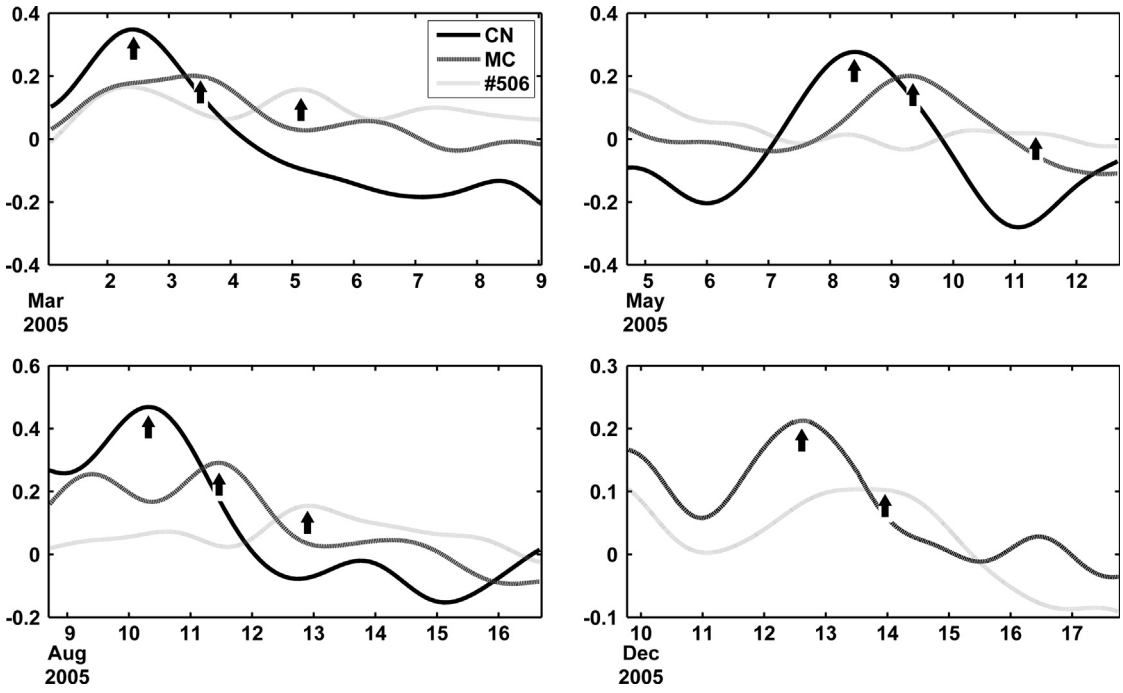

Fig. 17. Sub-inertial sea-level oscillations recorded in Cananéia (25°S) – CN, Macaé (22.4°S) – MC and Caravelas (station #506) for the same occasions described in Fig. 16. Arrows indicate correlated crests of shelf waves with an average 4-day period, taking 2–3 days to propagate from Cananéia to Caravelas. The sea level data for Cananeia and Macaé are provided by the Global Sea Level Observing System (GLOSS) – Brazil. Units are m.

on a few occasions geostrophic balance appears to be reached, as is the case in Fig. 16b (May 12th) and 16d (December 14th).

Sub-inertial sea level records from Cananéia (~1300 km to the south) and Macaé (~760 km to the south) confirm the propagation of shelf waves on all but one (Fig. 16b) of these occasions (Fig. 17). The r^2 between the sub-inertial sea level in Cananeia and at station #506 is 0.20, associated with a time lag of 2.4 days. The r^2 between the sea level in Macae and at station #506 is 0.15, with a time lag of 1.3 days. These results suggest that the speed of propagation is approximately 6 m s^{-1}, similar to what was found by Rahy (2006) for inner shelf wave speeds between São Sebastião and Cabo Frio (24°S).

This study is based on one of the longest current and sea level monitoring programs along the Brazilian coast. However, the time series analyzed are not long enough to resolve the interdecadal variability observed in the climatic and oceanographic systems, where the shortest interdecadal cycle is approximately 3 years (e.g., Melice and Servain, 2003; Evangelista et al., 2007; Labat, 2008). Evangelista et al. (2007) showed that coral growth in Abrolhos is modulated by air temperature, sea-surface temperature and precipitation following a cycle of 2–4 and 5–8 years. The observed trend in our dataset of decreasing frequency of negative (southbound) along-shore wind and currents might also be associated with these cycles. Therefore, the statistics presented herein should be interpreted with caution.

5. Summary and conclusions

The time variability of local and main forcing of circulation are described based on four years of wind, current and sea level data from two stations located on the inner shelf at Abrolhos Bank.

The along-shore circulation is mostly driven by the sub-inertial cross-shore pressure gradient induced by the along-shore winds with a marked seasonal cycle. South-southwestward along-shore currents occur between October and January, while stronger north-northeastward along-shore currents are observed in the fall and winter months. This reversal is driven by the N–S migration of the South Atlantic high between the summer and winter seasons. The sub-inertial along-shelf momentum balance is ageostrophic and mainly occurs between the wind and bottom stresses. The cross-shore pressure gradient is manly set up by along-shore winds.

The cross-shore circulation is manly forced by tides, and the sub-inertial flow is weak and restricted by the local topography. The sub-inertial cross-shore momentum balance in the region is essentially geostrophic, with smaller contributions from the cross-shore wind stress.

The passage of cold fronts is also important for the local circulation. Its effect can be perceived not only by the cold fronts that arrive in the region but also by the remote effect of the cold fronts that arrive in Cabo Frio, but these cold fronts are not capable of reaching Caravelas. The spectral analyses show a strong variability related to weather-band events. Our results also show an increasing frequency of the southern winds and, consequently, northward currents between 2002 and 2005 that are related to the number of fronts reaching a region 500 km southward. We suggest that this interannual variability is related to SOI events.

In addition, for the first time, we have shown that long-period shelf waves that propagate into the region change the inner shelf current field and sea level. These waves are created thousands kilometers south of Abrolhos Bank and can be described as the remote effect of the wind stress.

Finally, it is important to mention that the inner shelf region is the connection between land and the Abrolhos Coral Reef system, and a continuous monitoring program to better understand and monitor the circulation over this sector of the shelf would certainly benefit the Abrolhos system as a whole.

Acknowledgments

Mauro Cirano and Carlos Teixeira were supported by a CNPq Research grant. We thank Aracruz Cellulose and CEPEMAR for providing all datasets used in this paper.

References

Amorim, F.N., Cirano, M., Soares, I.D, Lentini, C.A.D., 2011. Coastal and shelf circulation in the vicinity of Camamu Bay (14°S), Eastern Brazilian Shelf. Continental Shelf Research 31 (2), 108–119.

Andutta, F.P., Miranda, L.B., 2013. Transport time scales in a well-mixed tropical estuary. Continental Shelf Research 70, 36–45.

Campos, E., 2006. Equatorward translation of the Vitoria Eddy in a numerical simulation. Geophysical Research Letters 33, L22607.

Castro, B.M., Lee, T.N., 1995. Wind-forced sea-level variability on the Southeast Brazilian Shelf. Journal of Geophysical Research 100 (C8), 16045–16056.

Chaves, R.R., 1999. Variabilidade da precipitação na região Sul do Nordeste e sua associação com padrões atmosféricos. MSc Thesis. Instituto Nacional de Pesquisas Espaciais, 159p.

Emery, W.J., Thomson, R.E., 1997. Data Analysis Methods in Physical Oceanography, 2nd ed., Elsevier Inc., New York.

Evangelista, H., Godiva, D., Sifeddine, A., Leão, Z.M.A.N., Rigozo, N.R., Segal, B., Ambrizzi, E.T, Kampel, M., Kikuchi, R.K.P., Le Cornec, F., 2007. Evidences linking ENSO and coral growth in the Southwestern-South Atlantic. Climate Dynamics 29 (7–8), 869–880.

Griffin, D.A., Middleton, J.H., Bode, L., 1987. The tidal and longer-period circulation of Capricornia, Southern Great Barrier Reef. Australian Journal of Marine & Freshwater Research 38 (4), 461–474.

Grinsted, A., Moore, J.C., Jevrejeva, S., 2004. Application of the cross wavelet transform and wavelet coherence to geophysical time series. Nonlinear Processes in Geophysics 11 (5–6), 561–566.

INPE, 2011. Climanálise – Boletim de Monitoramento e Análise Climática. Centro de Previsão de Tempo e Estudos Climáticos ⟨http://climanalise.cptec.inpe.br/~rclimanl/boletim/⟩.

Large, W.G., Pond, S., 1981. Open ocean momentum flux measurements in moderate to strong winds. Journal of Physical Oceanography 11, 324–336.

Labat, D., 2008. Wavelet analysis of the annual discharge records of the world's largest rivers. Advances in Water Resources 31 (1), 109–117.

Leão, Z.M.A.N., Ginsburg, R.N., 1997. Living reefs surrounded by siliciclastic sediments: the Abrolhos coastal reefs, Bahia, Brazil. In: Lessios, H.A., Macintyre, I.G. (Eds.), Proceedings of the 8th International Coral Reef Symposium, Panama, pp. 1767–1777.

Leipe, T., Knoppers, B., Marone, E., Camargo, R., 1999. Suspended matter transport in coral reef waters of the Abrolhos Bank, Brazil. Geo-Marine Letters 19 (3), 186–195.

Lentz, S., Guza, R.T., Elgar, S., Feddersen, F., Herbers, T.H.C., 1999. Momentum balances on the North Carolina inner shelf. Journal of Geophysical Research 104 (C8), 18205–18226.

Lentz, S.J., 1994. Current dynamics over the Northern California inner-shelf. Journal of Physical Oceanography 24 (12), 2461–2478.

Lessa, G.C., Cirano, M., 2006. On the circulation of a coastal channel within the Abrolhos coral-reef system – Southern Bahia (17°40′S), Brazil. Journal of Coastal Research 39, 450–453.

Liu, Y., Weisberg, R.H., 2005. Momentum balance diagnoses for the West Florida Shelf. Continental Shelf Research 25 (17), 2054–2074.

Melice, J.L., Servain, J., 2003. The tropical Atlantic meridional SST gradient index and its relationships with the SOI, NAO and Southern Ocean. Climate Dynamics 20 (5), 447–464.

Pawlowicz, R., Beardsley, B., Lentz, S., 2002. Classical tidal harmonic analysis including error estimates in MATLAB using T-TIDE. Computers and Geosciences 28 (8), 929–937.

Pereira, A.F., Belem, A.L, Castro, B.M., Geremias, R., 2005. Tide-topography interaction along the eastern Brazilian shelf. Continental Shelf Research 25 (12–13), 1521–1539.

Pereira, M.D., Siegle, E., Miranda, L.B., Schettini, C.A.F., 2010. Hidrodinâmica e transporte do material particulado em suspensão sazonal em um estuário dominado por maré: estuário de Caravelas (BA). Revista Brasileira de Geofísica 28 (3), 427–444.

Pezza, A.B., Ambrizzi, T., 2003. Variability of Southern Hemisphere cyclone and anticyclone behavior: further analysis. Journal of Climate 16 (7), 1075–1083.

Rahy, M.Q.T., 2006. Correntes Subinerciais e Ondas de Plataforma Continental Presentes na Costa Sudeste do Brasil. Master Thesis. Universidade de São Paulo, 90p.

Schettini, C.A.F., Miranda, L.B., 2010. Circulation and suspended matter transport in a tidally dominated estuary: Caravelas estuary, Bahia, Brazil. Brazilian Journal of Oceanography 58 (1), 1–11.

Schettini, C.A.F., Pereira, M.D., Siegle, E., Miranda, L.B., Silva, M.P., 2013. Residual fluxes of suspended sediment in a tidally dominated tropical estuary. Continental Shelf Research 70, 27–35.

Soutelino, R.G., Silveira, I.C.A., Gangopadhyay, A., Miranda, J.A., 2011. Is the Brazil Current eddy-dominated to the north of 20°S. Geophysical Research Letters 38 (3), L03607.